



Multi-parametric MRI of Kidney Disease Progression for Autosomal Recessive Polycystic Kidney Disease (ARPKD): Mouse Model and Initial Patient Results

Christina J. MacAskill¹, Bernadette O. Erokwu¹, Michael Markley², Ashlee Parsons³, Susan Farr¹, Yifan Zhang¹, Uyen Tran⁴, Yong Chen¹, Christian E. Anderson^{1,5}, Suraj Serai⁶, Erum A. Hartung⁷, Oliver Wessely⁴, Dan Ma^{1,5}, Katherine M. Dell^{3,8}, Chris A. Flask^{*,1,5,8}

¹Department of Radiology, Case Western Reserve University, Cleveland, OH, USA.

²Department of Radiology, University Hospitals Cleveland Medical Center, Cleveland, OH, USA.

³Center for Pediatric Nephrology, Cleveland Clinic Children's, Cleveland, OH, USA.

⁴Department of Cellular and Molecular Medicine, Lerner Research Institute, Cleveland Clinic Foundation, Cleveland, OH, USA

⁵Department of Biomedical Engineering, Case Western Reserve University, Cleveland, OH, USA.

⁶Department of Radiology, Children's Hospital of Philadelphia, Philadelphia, PA, USA.

⁷Department of Pediatrics, Children's Hospital of Philadelphia, Philadelphia, PA, USA.

⁸Department of Pediatrics, Case Western Reserve University, Cleveland, OH, USA.

Abstract

Background: Autosomal recessive polycystic kidney disease (ARPKD) is a rare but potentially lethal genetic disorder typically characterized by diffuse renal microcysts. Clinical trials for patients with ARPKD are not currently possible due to the absence of sensitive measures of ARPKD kidney disease progression and/or therapeutic efficacy.

Users may view, print, copy, and download text and data-mine the content in such documents, for the purposes of academic research, subject always to the full Conditions of use:http://www.nature.com/authors/editorial_policies/license.html#terms

***Corresponding author:** Chris A. Flask, Ph.D., Associate Professor, Departments of Radiology, Biomedical Engineering, and Pediatrics, Case Western Reserve University, 11100 Euclid Avenue, Bolwell Building, Room B115, caf@case.edu, PH: 216-844-4963. Author Contributions:

C.J.M provided substantial contributions to all aspects of this manuscript including the conception and design, acquisition of the data, analysis and interpretation of the data, and drafting and reviewing the manuscript. B.O.E, M.M., A.P., S.F., Y.Z, U.T., Y.C., C.E.A, O.W., D.M., K.M.D., and C.A.F. all contributed to the acquisition of the data. S.S. and E.A.H also contributed to the study conception and design. K.M.D and C.A.F. also contributed to the drafting and reviewing of the manuscript, and study conception and design.

Disclosure:

The authors declare no conflict of interest.

Category of Study:

Basic science.

Patient Consent:

All human imaging studies were performed in accordance with approved Institutional Review Board (IRB) protocols at the Cleveland Clinic and University Hospitals – Cleveland Medical Center. Informed written consent was obtained from all subjects before the MRI scans.

Methods: In this study, animal and human MRI scanners were used to obtain quantitative kidney T1 and T2 relaxation time maps for both excised kidneys from bpk and wild type (WT) mice as well as for a pediatric patient with ARPKD and a healthy adult volunteer.

Results: Mean kidney T1 and T2 relaxation times showed significant increases with age ($p < 0.05$) as well as significant increases in comparison to WT mice ($p < 2 \times 10^{-10}$). Significant or nearly significant linear correlations were observed for mean kidney T1 ($p = 0.030$) and T2 ($p = 0.054$) as a function of total kidney volume, respectively. Initial MRF assessments in a patient with ARPKD showed visible increases in both kidney T1 and T2 in comparison to the healthy volunteer.

Conclusions: These preclinical and initial clinical MRI studies suggest that renal T1 and T2 relaxometry may provide an additional outcome measure to assess cystic kidney disease progression in patients with ARPKD.

INTRODUCTION

Autosomal recessive polycystic kidney disease (ARPKD) is a rare but potentially lethal and rapidly progressing genetic disorder that affects approximately 1/20,000 children (1,2). ARPKD is typically characterized by diffuse renal microcysts caused by dilatations of the collecting tubules (2). ARPKD kidney disease progression results in declining kidney function at an early age. Of the 70% of patients with ARPKD that survive through the neonatal period (3), 40% progress to end-stage renal disease (ESRD) by 15 years of age (1,3). Importantly, there are currently no disease-specific therapies for patients with ARPKD beyond kidney transplant and dialysis (1,2,4). As a result, clinical management of chronic kidney disease (CKD) and its complications remains the primary treatment option for patients with ARPKD (1,2,4).

Several novel therapies have been recently shown to ameliorate kidney disease in animal models of ARPKD and other related ciliopathies (1,5–9). However, a major roadblock for implementing clinical trials in patients with ARPKD is the absence of sensitive measures of ARPKD kidney disease progression and / or therapeutic efficacy (1,4). Unfortunately, serum creatinine naturally increases with age in children (10,11). In addition, eGFR is relatively insensitive, especially for early-stage disease, and may not accurately reflect the severity of kidney damage (10,11). Furthermore, in many rare diseases such as ARPKD, there is significant variability in rates of GFR decline over time. A prior study examining kidney disease progression in patients with ARPKD found that rates of GFR decline were relatively modest and also highly variable across the patient population (mean 6% / year, range 1–10% / year) (12). Therefore, a clinical need exists to develop a safe and sensitive measure for kidney disease progression, and eventually therapeutic efficacy, for patients with ARPKD.

Magnetic Resonance Imaging (MRI) can be used to provide high-resolution kidney images in both patients and animal models. Importantly, MRI is capable of providing images with a variety of soft tissue contrasts that require no ionizing radiation or injectable contrast agent (13). MRI assessments of total kidney volume (TKV) has already been established as a marker for kidney disease progression in patients with autosomal dominant PKD (ADPKD). Unfortunately, unlike ADPKD, TKV for patients with ARPKD is not a reliable marker of disease since kidney size stabilizes over time as the normal renal parenchyma is replaced by

microcysts (1,14). Over the last decade, *quantitative* MRI techniques, such as diffusion MRI, arterial spin labeling (ASL), and MRI relaxometry (i.e., T1 and T2 mapping) have been used to noninvasively assess changes in renal microstructure, oxygenation, perfusion, and tissue composition for a variety of acute and chronic kidney diseases. However, most of these quantitative MRI techniques have not been thoroughly evaluated in either animal models or patients with ARPKD (1,15–19). In our initial work in the PCK rat model of ARPKD, we demonstrated that T2-weighted MRI reliably measured renal cystic burden with advancing cystic kidney disease (1). However, cystic kidney disease progression in the PCK rat is predominantly renal macrocysts. These macrocysts are in stark contrast to the diffuse renal microcysts typical of humans in ARPKD kidney disease. Therefore, in the current study we sought to evaluate the capability of T1 and T2 MRI to assess kidney progression in *ex vivo* kidneys from the bpk mouse model that exhibits diffuse renal cysts consistent with human ARPKD kidney disease, (9,20–22) with the overall hypothesis that kidney T1 and T2 MRI maps would provide sensitive assessments of cystic changes associated with progressive ARPKD kidney disease. In the second phase of this study, we obtained initial *in vivo* kidney T1 and T2 assessments in a patient with ARPKD and a healthy volunteer for comparison with the preclinical findings using a novel Magnetic Resonance Fingerprinting (MRF) technology.

METHODS

Preclinical MRI Assessments

Animal Models—All studies were conducted in accordance with approved Institutional Animal Care and use committee protocols at the Cleveland Clinic and Case Western Reserve University. Bpk mouse pups were euthanized at 8 (n=5), 14 (n=5), and 18 (n=3) days of age by exsanguination and the kidneys were excised and fixed in methanol. Kidneys from heterozygous age-matched littermates were also obtained as controls (8 (n=3), 14 (n=4), and 18 (n=5) days of age).

MRI Acquisitions—The preclinical MRI experiments were conducted on a 7.0 T Bruker Biospec small animal MRI scanner (Bruker, Inc., Billerica, MA). Both the left and right excised kidneys from each animal were scanned in centrifuge tubes filled with methanol. Each kidney sample was positioned with the kidney at isocenter in a 35-mm cylindrical transmit / receive volume coil to ensure uniform radiofrequency excitation. Axial T₂-weighted images were acquired with a multi-echo spin echo acquisition to position the slices for the quantitative MRI scans. High-resolution coronal T1 and T2 maps were then obtained for each mouse kidney. T1 data was obtained using a conventional spin echo acquisition with multiple repetition times (TR = 10,000 ms, 5,000 ms, 2,000 ms, 1,000 ms, 500 ms, and 300 ms) (23). Additional T1 imaging parameters were: echo time (TE) = 10.4 ms, slice thickness (TH) = 1.0 mm, 12 slices, field of view (FOV) = 35 × 35 mm, in-plane resolution = 0.273 × 0.273 mm/pixel, number of signal averages (NSA) = 1. Total acquisition time for the T1 measurement was 39 minutes and 54 seconds. T2 data was acquired with a multi-echo spin echo acquisition (12 echoes, TE = 52 ms, 63 ms, 73 ms, 83 ms, 94 ms, 104 ms, 115 ms, 125 ms, 136 ms, 146 ms, 157 ms, and 167 ms) (24). Detailed T2 imaging parameters were: TR = 2,000 ms, TH = 1.0 mm, 12 slices, FOV = 35 × 35 mm, in-plane

resolution = 0.273×0.273 mm/pixel. Total acquisition time for the T2 assessment was 17 minutes and 4 seconds.

Following completion of the preclinical MRI scans, representative kidneys from 8-day-old and 18-day-old bpk and age-matched WT littermates were paraffin-embedded. Five-micron sections centered at the renal hilum were obtained and stained with hematoxylin and eosin (H&E). Sections were visualized by light microscopy (2x magnification) and images captured using an attached digital camera and imported into Adobe Photoshop®.

Image and Statistical Analysis—*Ex vivo* MRI data was exported for offline analysis in Matlab (The Mathworks, Natick, MA). Quantitative T1 and T2 maps were obtained by voxel-wise linear least squared error fits of the imaging data to established mono-exponential models for magnetic relaxation (23,25,26). The resultant fits were visually inspected to ensure linearity of the data. A manual region-of-interest (ROI) analysis was performed on each imaging slice to calculate the mean and standard deviations for the T1 and T2 data for each kidney slice. The number of kidney voxels in each imaging slice was used to obtain weighted mean values over the set of imaging slices. An average of the left and right kidneys from each animal was completed. The total volume of each kidney was also calculated from the ROI analysis of the T2-weighted images.

Mean kidney T1 and T2 values for the bpk and control mice were compared across mouse strain and age using unpaired Student's t-tests. Pearson correlations were used to determine relationships between the mean T1 and T2 values with kidney volume. A two-tailed probability of 0.05 (α) was used to test for significance.

Human Kidney MRI Assessments

All human imaging studies were performed in accordance with approved Institutional Review Board (IRB) protocols at the Cleveland Clinic and University Hospitals – Cleveland Medical Center. For this initial study, we recruited one adolescent patient with ARPKD and one young adult volunteer subject (age=18). The human MRI studies were conducted using a Siemens Skyra 3.0 tesla MRI scanner (Siemens Healthineers, Erlangen, Germany).

Human Kidney MRI Experiments—Each subject was scanned in the supine position using both a body array and spine array receiver coils to ensure uniform image quality over the subject's kidneys. Initial localizer HASTE (Half-Fourier Acquisition Single-shot Turbo spin Echo) images were acquired during instructed breathholds in all three imaging planes to obtain anatomic images of both the left and right kidneys for accurate slice positioning in later acquisitions. T1 and T2 MRI data for each kidney was then was acquired for each kidney using a rapid Magnetic Resonance Fingerprinting (MRF) acquisition. The method as demonstrated by Chen, Y. *et al.* was adapted for use in the abdomen with the following parameters: TR = 5.74 ms, TE = 1.00 ms, flip angle range = 5–12°, TH = 6.0 mm, field of view (FOV) = 400 × 400 mm, in-plane resolution = 1.3×1.3 mm/pixel, 1728 MRF images, acquisition time = 15 seconds (27). Each MRF acquisition resulted in co-registered T1 and T2 maps for a single imaging slice (27). Each MRF imaging slice was positioned parallel to the long axis of each kidney. Three oblique coronal MRF images were acquired for both the left and right kidneys.

Human Image and Statistical Analysis—The human MRI data was exported for offline analysis in Matlab (The Mathworks, Natick, MA). Quantitative T1 and T2 maps for the MRF acquisitions were obtained by voxel-wise matching of the acquired MRF image profiles to the MRF dictionary as described previously (27,28). No other statistical calculations were completed for these proof-of-concept human studies.

RESULTS

Representative maps of renal T1 and T2 relaxation times as well as H&E-stained sections for an 18-day-old bpk mouse (**A, B, C**), an 8-day-old bpk mouse (**D, E, F**), and an 18-day-old WT mouse (**G, H, I**) are shown in Figure 1, respectively. Note the diffuse cystic architecture as well as the increased cystic burden and kidney volume for the bpk kidneys. The kidneys from the bpk mice also show visible increases in the renal T1 and T2 MRI values between 8-days-of-age and 18-days-of-age as expected due to cystic kidney disease progression.

Mean kidney T1 and T2 values for each age group for both bpk and wild type mice plotted as a function of age are shown in Figure 2. The mean T1 and T2 values for the bpk kidneys were all significantly increased in comparison to the WT kidneys at all timepoints with respect to age ($p < 2 \times 10^{-10}$). For the bpk mice, significant increases in mean kidney T1 and T2 values were also observed for the older kidneys (T1: 8 vs. 18 days, $p = 0.018$; T2: 8 vs. 14 days, $p = 0.0002$ and 8 vs. 18 days, $p = 0.0009$). In contrast, the corresponding mean kidney values for the WT mice either decreased with age (T1: 8 vs. 18 days, $p = 0.03$) or did not change significantly (T2: all WT mice, $p > 0.13$). Histograms showing the voxel-wise compilation of kidney T1 and T2 values for bpk and WT control mice as a function of age are shown in Supplementary Figure 1.

Mean kidney T1 and T2 values for bpk mice and WT control mice are also plotted as a function of total kidney volume (Figure 3 A, B). As expected, T1 and T2 values for the bpk kidneys increased with increasing kidney volume. The mean kidney T1 values for the bpk mice ($n=13$) resulted in a significant linear correlation with total kidney volume ($R = 0.60$, $p = 0.030$). Mean kidney T2 values trended towards a significant correlation with total kidney volume (T2: $R = 0.55$, $p = 0.054$). No significant correlations were observed between the MRI metrics and total kidney volume for the WT kidneys.

Initial T1 and T2 maps for both the healthy young adult volunteer and the adolescent patient with ARPKD are shown in Figure 4. Note the obvious diffuse cystic architecture as well as the obvious size increases for the kidneys of the patient with ARPKD. The kidneys from the patient with ARPKD shows visible increases in T1 and T2 in comparison to the kidneys from the healthy volunteer. Overall, these initial human MRI assessments for ARPKD kidney disease are consistent with the preclinical imaging findings in Figures 1–3.

DISCUSSION

In this study, we evaluated the capability of quantitative MRI techniques to assess cystic burden in ARPKD kidney disease. In particular, we evaluated the capability of mean kidney T1 and T2 MRI to quantify cystic kidney disease progression in a well-established ARPKD

animal model that exhibits progressively increasing diffuse renal microcysts. We also performed initial proof-of-concept studies in a patient with ARPKD and a healthy volunteer. The mean kidney T1 and T2 for the bpk kidneys increased significantly with age consistent with histology and were significantly higher than for the WT kidneys (Figures 1 and 2). In addition, both of these MRI metrics exhibited significant (T1) or nearly significant (T2) correlations with total kidney volume (Figure 3). Most importantly, the initial human MRI results were consistent with these preclinical MRI assessments (Figure 4). Therefore, while additional longitudinal imaging studies in patients with ARPKD will need to be conducted to more fully evaluate the sensitivity and specificity of these MRI techniques in comparison to conventional clinical measures of kidney function (e.g., serum creatinine), these preclinical and initial clinical MRI results suggest that T1 and T2 MRI could be used to assess cystic kidney progression in patients with ARPKD.

The MRI methods used in this study have a number of advantages for eventual studies in patients with ARPKD. First, these MRI techniques are non-invasive and do not require any injectable MRI contrast agent making these methods safe for longitudinal studies for pediatric and adult patients with advanced kidney disease (13). Second, these MRI methods are quantitative and therefore provide an objective outcome measure that could be used in future clinical trials. Third, the clinical MRF techniques used herein require very short acquisition times (~15 seconds) resulting in reduced respiratory motion artifacts, potentially eliminating the need for deep sedation or general anesthesia for pediatric patients. Fourth, T1 and T2 MRI techniques are available on virtually all modern human MRI scanners. For example, T1 MRI assessments have been used in numerous MRI studies of the heart, lung, liver, and other organs (29–35). As such, these methods could be rapidly implemented in multi-center clinical trials to evaluate new therapies for ARPKD.

The MRF acquisition used to obtain the initial human kidney T1 and T2 maps shown in Figure 4 also provides multiple benefits for future human ARPKD studies. This methodology was initially described in 2013 and uses rapid a priori variation in the MRI acquisition parameters (e.g., excitation flip angle) to generate tissue-specific MRF signal evolution profiles. These profiles are then matched to the best-fitting theoretical signal evolution profile in the MRF dictionary to obtain simultaneous estimates of the T1 and T2 relaxation times for each image voxel. Multiple studies have previously shown that MRF is inherently resistant to motion artifacts and results in accurate and reproducible assessments of T1 and T2 relaxation times for brain, kidney, liver, and prostate imaging applications (27,36–39). For the MRF implementation used herein, we utilized a low tip angle MRF acquisition which provides accurate T1 and T2 estimates without the need for additional scans to compensate for B1 heterogeneities (27,38). The lower tip angles also limit the radiofrequency energy deposition to the subject. As this MRF acquisition was completed in a single 15-second breathhold for each imaging slice, the T1 and T2 relaxation time maps were free of respiratory motion artifacts. These T1 and T2 MRI assessments may also be combined with renal perfusion assessments or other imaging methodologies to more thoroughly characterize ARPKD kidney disease progression (34).

While these preclinical and initial clinical MRI studies show promise for the use of quantitative MRI methods to assess ARPKD kidney disease progression, this study also has

several important limitations. The primary limitation for the preclinical portion of this study is that the bpk and WT kidneys were scanned *ex vivo*. It is well established that blood flow can significantly alter the *in vivo* kidney T1 and T2 values (40). As such, the addition of a renal blood MRI signal would likely alter the mean kidney T1 and T2 values for both the bpk and WT mice. However, while the absolute values for the *ex vivo* kidney T1 and T2 times may be somewhat different from *in vivo* values, the differences in T1 and T2 values between the bpk and WT mice as well as the changes in the kidney T1 and T2 values with age remain significant. Further, as the long-term goal of this study is to develop MRI markers of cystic kidney disease progression in patients with ARPKD, this *ex vivo* imaging approach allows these T1 and T2 MRI techniques to be initially evaluated in a very controlled environment with limited impact of known variables such as hydration status, cardiac output, and respiratory motion that can create confounds with the cystic disease information in the MRI data. Scanning these kidneys *ex vivo* also allows multiple MRI parameters (T1 and T2) to be acquired with very high resolution and accuracy. As such, the conventional spin echo methods used in this study to generate the *ex vivo* T1 and T2 maps for the bpk and WT kidneys require significant acquisition times (total scan time = ~1 hour) that are not practical for *in vivo* studies of bpk mice with advanced kidney disease. Ultimately, these *ex vivo* preclinical MRI results are consistent with both histology (Figure 1) as well as initial *in vivo* human MRI assessments (Figure 4). As such, these *ex vivo* MRI findings help support the notion that T1 and T2 MRI assessments may be useful to assess ARPKD kidney disease progression in patients.

The primary limitation for the clinical MRI studies is the small sample size. While additional patient scans are certainly needed, these proof-of-concept human imaging studies establish that obtaining high resolution, quantitative kidney T1 and T2 MRI maps in a practical timeframe with no sedation in a pediatric patient is feasible. Most importantly, these and any other MRI metrics will need to be compared with conventional measures of renal function (e.g., serum creatinine and albumin) in both cross-sectional and longitudinal imaging studies in order to evaluate the utility of these MRI techniques to assess ARPKD kidney disease progression in multi-center clinical trials.

In conclusion, this preclinical and initial clinical study suggests that MRI-based kidney T1 and T2 mapping could be used as a non-invasive imaging assessment of ARPKD kidney disease progression. Future longitudinal MRI / MRF studies in patients with ARPKD will further evaluate the sensitivity, specificity, and reproducibility of these MRI techniques to detect and stage ARPKD kidney disease. If successful, these non-invasive, quantitative MRI techniques could eventually be used as an outcome measure for clinical trials evaluating novel therapeutics aimed at limiting or preventing ARPKD kidney disease progression.

Supplementary Material

Refer to Web version on PubMed Central for supplementary material.

ACKNOWLEDGEMENTS

The authors would like to thank Michael Kavran and other staff of the Imaging Research Core at CWRU for their timely support.

Statement of financial support:

This research was supported by NIH / NIDDK R01 DK114425 and the PKD Foundation. In addition, this work utilized the imaging capabilities for the Imaging Research Core for the Case Comprehensive Cancer Center (P30 CA043703), the Digestive Diseases Research Core Center (P30 DK097948), and the Cystic Fibrosis Foundation Research Development Program.

REFERENCES

1. Erokwu BO, Anderson CE, Flask CA, Dell KM. Quantitative magnetic resonance imaging assessments of autosomal recessive polycystic kidney disease progression and response to therapy in an animal model. *Pediatr Res* [Internet]. 2018;83(5):1067–74. Available from: 10.1038/pr.2018.24
2. Macrae Dell K. The Spectrum of Polycystic Kidney Disease in Children. *Adv Chronic Kidney Dis* [Internet]. 2011;18(5):339–47. Available from: 10.1053/j.ackd.2011.05.001
3. Roy S, Dillon MJ, Trompeter RS, Barratt TM. Autosomal recessive polycystic kidney disease: long-term outcome of neonatal survivors. *Pediatr Nephrol* [Internet]. 1997 6 [cited 2018 Jul 23];11(3):302–6. Available from: <http://www.ncbi.nlm.nih.gov/pubmed/9203177>
4. Guay-Woodford LM, Bissler JJ, Braun MC, Bockenbauer D, Cadnapaphornchai MA, Dell KM, et al. Consensus expert recommendations for the diagnosis and management of autosomal recessive polycystic kidney disease: report of an international conference. *J Pediatr* [Internet]. 2014 9 [cited 2018 Jul 23];165(3):611–7. Available from: <http://www.ncbi.nlm.nih.gov/pubmed/25015577>
5. Ta MHT, Schwensen KG, Foster S, Korgaonkar M, Ozimek-Kulik JE, Phillips JK, et al. Effects of TORC1 Inhibition during the Early and Established Phases of Polycystic Kidney Disease. *PLoS One* [Internet]. 2016 [cited 2018 Jul 23];11(10):e0164193 Available from: <http://www.ncbi.nlm.nih.gov/pubmed/27723777> [PubMed: 27723777]
6. Franke M, Baeßler B, Vechtel J, Dafinger C, Höhne M, Borgal L, et al. Magnetic resonance T2 mapping and diffusion-weighted imaging for early detection of cystogenesis and response to therapy in a mouse model of polycystic kidney disease. *Kidney Int* [Internet]. 2017 12 1 [cited 2018 Jul 23];92(6):1544–54. Available from: <https://www.sciencedirect.com/science/article/pii/S0085253817303940?via%3Dihub>
7. Ta MHT, Rao P, Korgaonkar M, Foster SF, Peduto A, Harris DCH, et al. Pyrrolidine dithiocarbamate reduces the progression of total kidney volume and cyst enlargement in experimental polycystic kidney disease. *Physiol Rep* [Internet]. 2014 12 1 [cited 2018 Jul 23];2(12). Available from: <http://www.ncbi.nlm.nih.gov/pubmed/25501440>
8. Aihara M, Fujiki H, Mizuguchi H, Hattori K, Ohmoto K, Ishikawa M, et al. Tolvaptan delays the onset of end-stage renal disease in a polycystic kidney disease model by suppressing increases in kidney volume and renal injury. *J Pharmacol Exp Ther* [Internet]. 2014 5 1 [cited 2018 Jul 23];349(2):258–67. Available from: <http://www.ncbi.nlm.nih.gov/pubmed/9864265>
9. Nauta J, Ozawa Y, Sweeney WE, Rutledge JC, Avner ED. Renal and biliary abnormalities in a new murine model of autosomal recessive polycystic kidney disease. *Pediatr Nephrol* [Internet]. 1993 4 [cited 2018 Jul 23];7(2):163–72. Available from: <http://www.ncbi.nlm.nih.gov/pubmed/8476712>
10. Schwartz GJ, Muñoz A, Schneider MF, Mak RH, Kaskel F, Warady BA, et al. New Equations to Estimate GFR in Children with CKD. *J Am Soc Nephrol* [Internet]. 2009 3 [cited 2020 Jan 13];20(3):629–37. Available from: <http://www.jasn.org/lookup/doi/10.1681/ASN.2008030287>
11. Levey AS, Stevens LA, Schmid CH, Zhang Y, Lucy, Castro AF, Feldman HI, et al. A New Equation to Estimate Glomerular Filtration Rate. *Ann Intern Med* [Internet]. 2009 5 5 [cited 2020 Jan 13];150(9):604 Available from: <http://annals.org/article.aspx?doi=10.7326/0003-4819-150-9-200905050-00006>
12. Dell KM, Matheson M, Hartung EA, Warady BA, Furth SL. Chronic Kidney Disease in Children (CKiD) Study on behalf of the CKD in C (CKiD). *Kidney Disease Progression in Autosomal Recessive Polycystic Kidney Disease*. *J Pediatr* [Internet]. 2016 4 [cited 2018 Jul 23];171:196–201.e1. Available from: <http://www.ncbi.nlm.nih.gov/pubmed/26831744>
13. Fraum TJ, Ludwig DR, Bashir MR, Fowler KJ. Gadolinium-based contrast agents: A comprehensive risk assessment. *J Magn Reson Imaging* [Internet]. 2017 8 [cited 2018 Jul 25];46(2):338–53. Available from: <http://www.ncbi.nlm.nih.gov/pubmed/28083913>

14. Avni FE, Guissard G, Hall M, Janssen F, DeMaertelaer V, Rypens F. Hereditary polycystic kidney diseases in children: changing sonographic patterns through childhood. *Pediatr Radiol* [Internet]. 2002 3 [cited 2018 Jul 23];32(3):169–74. Available from: <http://www.ncbi.nlm.nih.gov/pubmed/12164348>
15. Xu X, Fang W, Ling H, Chai W, Chen K. Diffusion-weighted MR imaging of kidneys in patients with chronic kidney disease: initial study. *Eur Radiol* [Internet]. 2010 4 30 [cited 2018 Jul 23];20(4):978–83. Available from: <http://link.springer.com/10.1007/s00330-009-1619-8>
16. Zhao J, Wang ZJ, Liu M, Zhu J, Zhang X, Zhang T, et al. Assessment of renal fibrosis in chronic kidney disease using diffusion-weighted MRI. *Clin Radiol* [Internet]. 2014 11 1 [cited 2018 Jul 23];69(11):1117–22. Available from: <https://www.sciencedirect.com/science/article/pii/S0009926014003213?via%3Dihub>
17. Zheng Z, Shi H, Zhang J, Zhang Y. Renal water molecular diffusion characteristics in healthy native kidneys: assessment with diffusion tensor MR imaging. *PLoS One* [Internet]. 2014 [cited 2018 Jul 23];9(12):e113469 Available from: <http://www.ncbi.nlm.nih.gov/pubmed/25470776>
18. Zhang JL, Morrell G, Rusinek H, Sigmund EE, Chandarana H, Lerman LO, et al. New magnetic resonance imaging methods in nephrology. *Kidney Int* [Internet]. 2014 4 [cited 2018 Jul 23];85(4):768–78. Available from: <http://www.ncbi.nlm.nih.gov/pubmed/24067433>
19. Lu L, Sedor JR, Gulani V, Schelling JR, O'Brien A, Flask CA, et al. Use of diffusion tensor MRI to identify early changes in diabetic nephropathy. *Am J Nephrol* [Internet]. 2011 [cited 2018 Jul 23];34(5):476–82. Available from: <http://www.ncbi.nlm.nih.gov/pubmed/22024476>
20. Veizis EI, Carlin CR, Cotton CU. Decreased amiloride-sensitive Na absorption in collecting duct principal cells isolated from BPK ARPKD mice. *Am J Physiol Ren Physiol* [Internet]. 2004 [cited 2018 Jul 23];286:244–54. Available from: <http://www.ajprenal.org>
21. Guay-Woodford LM, Bryda EC, Christine B, Lindsey JR, Collier WR, Avner ED, et al. Evidence that two phenotypically distinct mouse PKD mutations, bpk and jcpk, are allelic. *Kidney Int* [Internet]. 1996 10 1 [cited 2018 Jul 23];50(4):1158–65. Available from: <https://www.sciencedirect.com/science/article/pii/S0085253815597172>
22. Guay-Woodford LM, Wright CJ, Walz G, Churchill GA. Quantitative trait loci modulate renal cystic disease severity in the mouse bpk model. *J Am Soc Nephrol* [Internet]. 2000 7 [cited 2018 Jul 23];11(7):1253–60. Available from: <http://www.ncbi.nlm.nih.gov/pubmed/10864581>
23. Juwhanliu AK, Nieminen A, Koenig. Calculation of T1, T2, and Proton Spin Density Images in Nuclear Magnetic Resonance Imaging. *J Magn Reson* [Internet]. 1989 [cited 2018 Jul 24];95–110. Available from: https://ac.els-cdn.com/0022236489903235/1-s2.0-0022236489903235-main.pdf?_tid=ee9c9d9e-0a39-45ae-ac67-e4b9f23289e6&acdnat=1532465035_6170064d97b4773600a2eec0fe3f4f6e
24. Liney GP, Knowles AJ, Manton DJ, Turnbull LW, Blackband SJ, Horsman A. Comparison of conventional single echo and multi-echo sequences with a fast spin-echo sequence for quantitative T2 mapping: Application to the prostate. *J Magn Reson Imaging* [Internet]. 1996 7 [cited 2018 Jul 24];6(4):603–7. Available from: <http://doi.wiley.com/10.1002/jmri.1880060408>
25. Jacobs MA, Ouwerkerk R, Petrowski K, Macura KJ. Diffusion-weighted imaging with apparent diffusion coefficient mapping and spectroscopy in prostate cancer. *Top Magn Reson Imaging* [Internet]. 2008 12 [cited 2018 Jul 23];19(6):261–72. Available from: <http://www.ncbi.nlm.nih.gov/pubmed/19512848>
26. Lee DK, Song YK, Park BW, Cho HP, Yeom JS, Cho G, et al. The robustness of T₂ value as a trabecular structural index at multiple spatial resolutions of 7 Tesla MRI. *Magn Reson Med* [Internet]. 2018 4 15 [cited 2018 Jul 24]; Available from: <http://www.ncbi.nlm.nih.gov/pubmed/29656389>
27. Chen Y, Chen MH, Baluyot KR, Potts TM, Jimenez J, Lin W. MR fingerprinting enables quantitative measures of brain tissue relaxation times and myelin water fraction in the first five years of life. *Neuroimage*. 2019 2 1;186:782–93. [PubMed: 30472371]
28. Ma D, Gulani V, Seiberlich N, Liu K, Sunshine JL, Duerk JL, et al. Magnetic resonance fingerprinting. *Nature* [Internet]. 2013 3 14 [cited 2018 Jul 25];495(7440):187–92. Available from: <http://www.nature.com/articles/nature11971>

29. Everett RJ, Stirrat CG, Semple SIR, Newby DE, Dweck MR, Mirsadraee S. Assessment of myocardial fibrosis with T1 mapping MRI. Vol. 71, *Clinical Radiology*. W.B. Saunders Ltd; 2016 p. 768–78.
30. Messroghli DR, Radjenovic A, Kozerke S, Higgins DM, Sivananthan MU, Ridgway JP. Modified Look-Locker inversion recovery (MOLLI) for high-resolution T1 mapping of the heart. *Magn Reson Med* [Internet]. 2004 7 [cited 2019 Dec 9];52(1):141–6. Available from: <http://doi.wiley.com/10.1002/mrm.20110>
31. Dasenbrook EC, Lu L, Donnola S, Weaver DE, Gulani V, Jakob PM, et al. Normalized T1 Magnetic Resonance Imaging for Assessment of Regional Lung Function in Adult Cystic Fibrosis Patients - A Cross-Sectional Study. *PLoS One*. 2013 9 25;8(9).
32. Ramachandran P, Serai SD, Veldtman GR, Lang SM, Mazur W, Trout AT, et al. Assessment of liver T1 mapping in fontan patients and its correlation with magnetic resonance elastography-derived liver stiffness. *Abdom Radiol*. 2019;
33. Haimerl M, Verloh N, Zeman F, Fellner C, Müller-Wille R, Schreyer AG, et al. Assessment of clinical signs of liver cirrhosis using T1 mapping on Gd-EOB-DTPA-enhanced 3T MRI. *PLoS One*. 2013 12 31;8(12).
34. Gillis KA, McComb C, Patel RK, Stevens KK, Schneider MP, Radjenovic A, et al. Non-Contrast Renal Magnetic Resonance Imaging to Assess Perfusion and Corticomedullary Differentiation in Health and Chronic Kidney Disease. *Nephron* [Internet]. 2016 [cited 2018 Dec 4];133(3):183–92. Available from: <https://www.karger.com/Article/FullText/447601>
35. Hamlin SA, Henry TS, Little BP, Lerakis S, Stillman AE. Mapping the Future of Cardiac MR Imaging: Case-based Review of T1 and T2 Mapping Techniques I. *RadioGraphics* [Internet]. 2014 [cited 2018 Jul 23];34(6):1594–611. Available from: www.rsna.org/rsnarights.
36. Gao Y, Chen Y, Ma D, Jiang Y, Herrmann KA, Vincent JA, et al. Preclinical MR fingerprinting (MRF) at 7 T: effective quantitative imaging for rodent disease models. *NMR Biomed* [Internet]. 2015 3 [cited 2018 Jul 25];28(3):384–94. Available from: <http://www.ncbi.nlm.nih.gov/pubmed/25639694>
37. Ma D, Gulani V, Seiberlich N, Liu K, Sunshine JL, Duerk JL, et al. Magnetic resonance fingerprinting. *Nature*. 2013 3 14;495(7440):187–92. [PubMed: 23486058]
38. Chen Y, Jiang Y, Pahwa S, Ma D, Lu L, Twieg MD, et al. MR Fingerprinting for Rapid Quantitative Abdominal Imaging. *Radiology* [Internet]. 2016 4 [cited 2019 Dec 9];279(1):278–86. Available from: <http://pubs.rsna.org/doi/10.1148/radiol.2016152037>
39. Yu AC, Badve C, Ponsky LE, Pahwa S, Dastmalchian S, Rogers M, et al. Development of a Combined MR Fingerprinting and Diffusion Examination for Prostate Cancer. *Radiology* [Internet]. 2017 6 [cited 2019 Dec 9];283(3):729–38. Available from: <http://pubs.rsna.org/doi/10.1148/radiol.2017161599>
40. Pohlmann A, Arakelyan K, Hentschel J, Cantow K, Flemming B, Ladwig M, et al. Detailing the relation between renal T2* and renal tissue pO2 using an integrated approach of parametric magnetic resonance imaging and invasive physiological measurements. *Invest Radiol* [Internet]. 2014 8 [cited 2018 Dec 4];49(8):547–60. Available from: <https://insights.ovid.com/crossref?an=00004424-201408000-00007>

Impact Questions:

- A major roadblock for implementing clinical trials in patients with ARPKD is the absence of sensitive measures of ARPKD kidney disease progression and / or therapeutic efficacy
- A clinical need exists to develop a safe and sensitive measure for kidney disease progression, and eventually therapeutic efficacy, for patients with ARPKD
- Mean kidney T1 and T2 MRI relaxation times showed significant increases with age ($p < 0.05$) as well as significant increases in comparison to WT mice ($p < 2 \times 10^{-10}$), indicating T1 and T2 may provide sensitive assessments of cystic changes associated with progressive ARPKD kidney disease
- This preclinical and initial clinical study suggests that MRI-based kidney T1 and T2 mapping could be used as a non-invasive assessment of ARPKD kidney disease progression
- These non-invasive, quantitative MRI techniques could eventually be used as an outcome measure for clinical trials evaluating novel therapeutics aimed at limiting or preventing ARPKD kidney disease progression

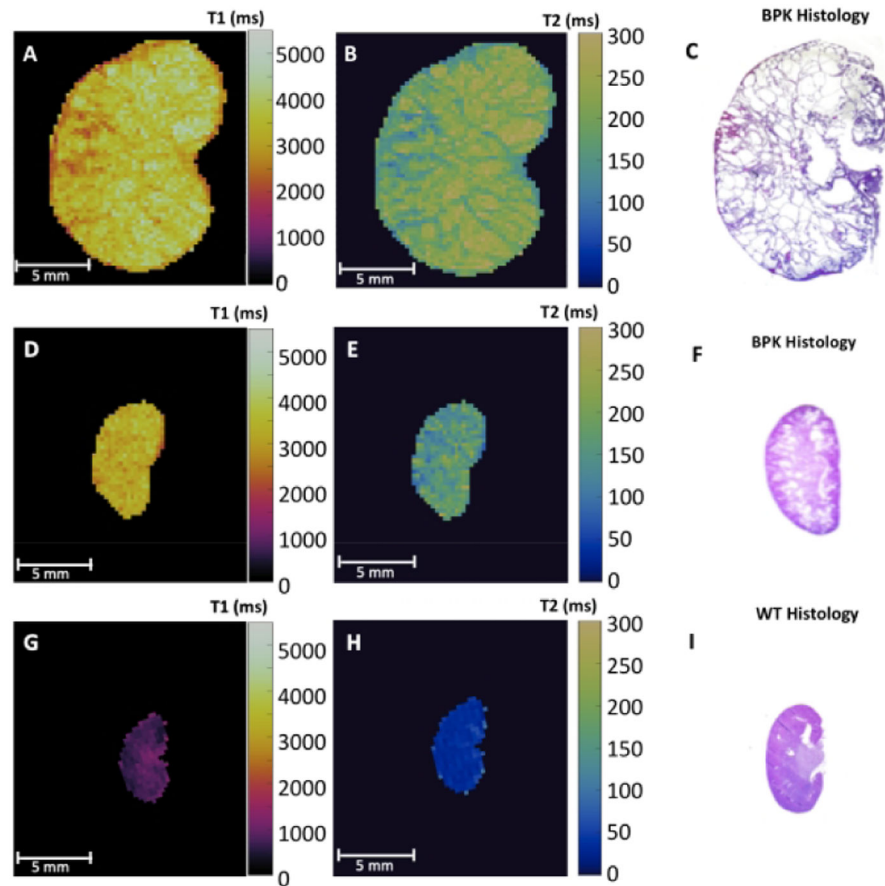


Figure 1: Representative ex vivo T1 and T2 relaxation time maps and corresponding H&E stained sections of (A,B,C) 18-day-old bpk mouse kidney, (D,E,F) 8-day-old bpk mouse kidney, and (G,H,I) 18-day-old WT mouse kidney. Note the visibly increased renal T1 and T2 values for the bpk kidneys over time in comparison to the WT kidney.

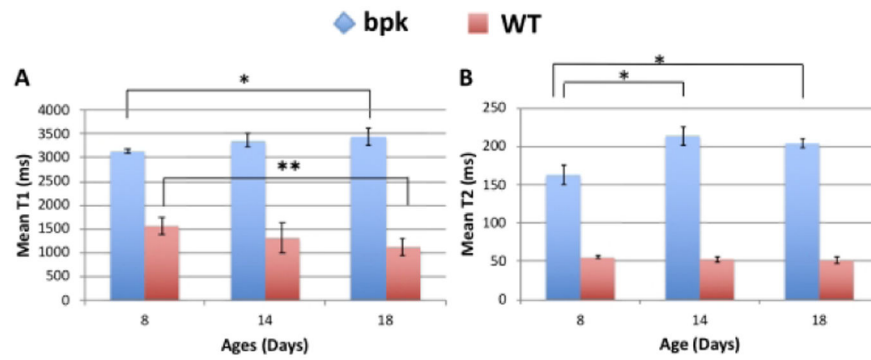


Figure 2:

Comparison of mean renal **A)** T1 and **B)** T2 relaxation time for bpk and WT mice at 8 days, 14 days, 18 days of age. Bpk mouse kidneys exhibit progressive increases in T1 and T2 with age (* $p < 0.02$). In contrast, WT mice show no change in T2 and a reduction in T1 with age (** $p = 0.03$). Mean renal T1 and T2 values were also significantly increased for bpk mice in comparison to WT control mice at all ages ($p < 2 \times 10^{-10}$).

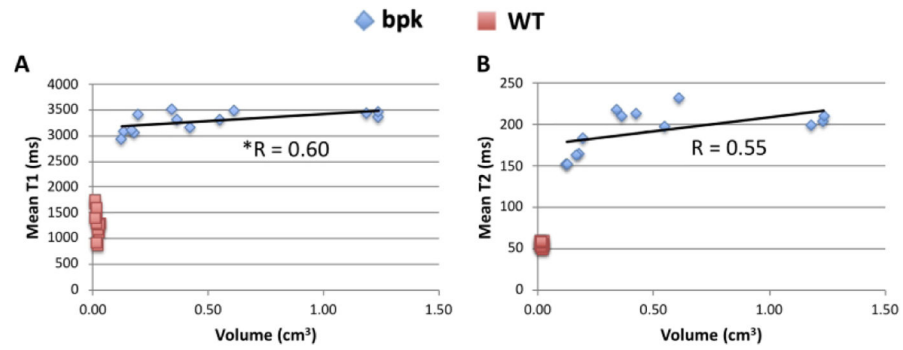


Figure 3: Scatterplots of mean renal **A)** T1 and **B)** T2 relaxation time for bpk mice and WT mice as a function of total kidney volume. Mean renal T1 ($R=0.60$, $*p=0.030$) and T2 ($R=0.55$, $p=0.054$) show significant (T1) or nearly significant (T2) correlations with kidney volume. No significant correlations were observed for the WT mice.

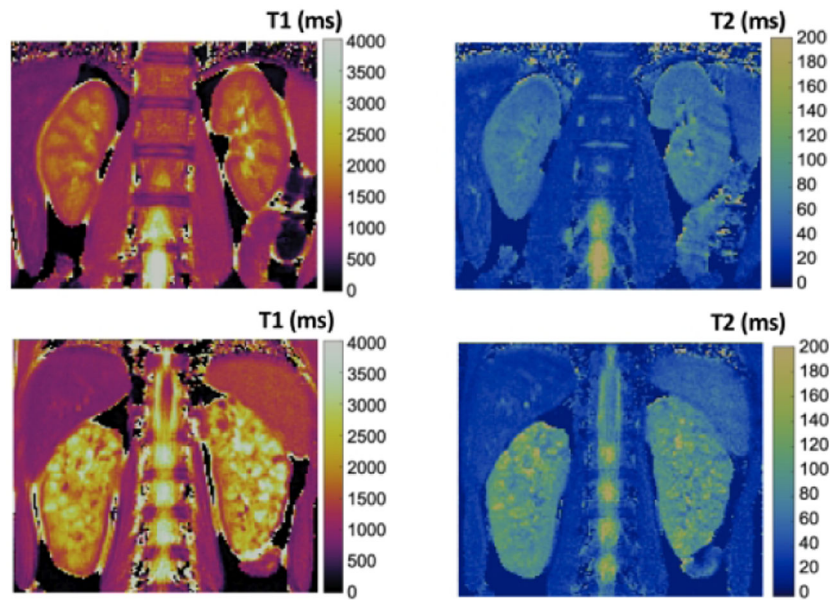


Figure 4: Initial renal T1 (left column) and T2 (right column) relaxation time maps from a healthy young adult volunteer (top row) and a pediatric patient with ARPKD (bottom row). Note the visible increases in T1 and T2 for the patient with ARPKD consistent with the *ex vivo* bpk kidney MRI results.